ISSN 0031-918X, Physics of Metals and Metallography, 2024, Vol. 125, No. 11, pp. 1175–1182. © The Author(s), 2024. This article is an open access publication.

STRUCTURE, PHASE TRANSFORMATIONS, AND DIFFUSION

Metastable Nanoprecipitates in Alloys: Phenomenology and Atomistic Simulation

I. K. Razumov[a, *] **and Yu. N. Gornostyrev**[a]
[a] *Mikheev Institute of Metal Physics, Ural Branch of the Russian Academy of Sciences, Ekaterinburg, 620108 Russia*
**e-mail: rik@imp.uran.ru*

Received June 20, 2024; revised July 3, 2024; accepted July 8, 2024

Abstract—Metastable disperse states arising from decomposition in alloys are of considerable interest and have an important practice-related significance, providing high strength properties. Recently, the stabilization mechanism of disperse states through the formation of a shell enriched in alloying elements has attracted special attention. The paper presents a concise overview of the theoretical concepts pertaining to the formation and stabilization of disperse states in alloys, along with recent findings from first-principles atomistic simulations of Al–Cu–X, Fe–Cu–X, and Al–Sc–Zr alloys, wherein precipitates with a core–shell structure have been observed. Furthermore, the paper addresses the conditions of kinetic and thermodynamic stabilization of precipitates in relation to coalescence processes during annealing.

Keywords: disperse states in alloys, spinodal decomposition, segregations, precipitates, first-principle calculations, molecular dynamics, Monte Carlo simulation

DOI: 10.1134/S0031918X24601719

1. INTRODUCTION

One method of creating new materials is through the formation of specific structures that impart the requisite properties. It is of particular interest to consider bulk nanostructured materials comprising structural elements with a characteristic size of approximately 100 nm, which offer the potential to implement unusual physical and mechanical properties. Despite significant advancements in the understanding of the intrinsic properties of nanomaterials over the past few decades, the precise physical mechanisms that govern the formation and stability of their microstructure remain a topic of ongoing discussion [3–7].

The formation of nanoscale microstructures during quenching can be attributed to the stabilization of the incomplete stage of phase transformations. In such cases, a regular tweed structure with a pronounced short-range can be observed as a consequence of spinodal decomposition [8]. Known examples of such structural states include stripe magnetic domains [9], antiphase domain structure in tetragonal ordered alloys [10], and lamellar martensitic [11, 12] or pearlitic [13] structure in steels. In this case, a significant role in the stabilization of structural states is played by long-range (elastic and magnetic) interactions [6].

There is another, actively investigated class of materials, whose structure is characterized by the presence of stable or metastable nanoscale precipitates in the alloy matrix [7]. Examples of this kind of heterogeneous state include Guinier–Preston pre-precipitates (zones) (or *K*-states [14]) in aluminum alloys [15, 16], as well as the formation of athermal ω-phase in Ti and Zr alloys [17], as well as in the Cu–Zn system [18], formation of Cu precipitates in Fe [19], Pb in Al [20], and Al_3Sc phase in Al [21].

The traditional phase transformation theories encounter significant challenges when attempting to explain the stability of the structural states that are formed in these cases (for further details, refer to the discussion in [5]). In the context of approaches that consider the volumetric and surface energies of precipitates, the nuclei of a new phase either dissolve (if their size is below the critical size) or grow indefinitely [8, 14, 22].

To explain the formation of stable disperse states, various generalizations of classical concepts have been proposed, which take into account the relief of the elastic energy of the alloy due to loss of coherence at the boundary of precipitates [5, 14, 23], segregation of impurities at phase interfaces [23–25], and lattice misfit in the matching of precipitates and the matrix [26].

In recent years, there has been a notable increase in research activity focused on the formation and stability of disperse composite precipitates with a core–shell structure. Examples of such systems include Al–Cu–(Mg,Zr) [27, 28], Fe–Cu–Ni–Al

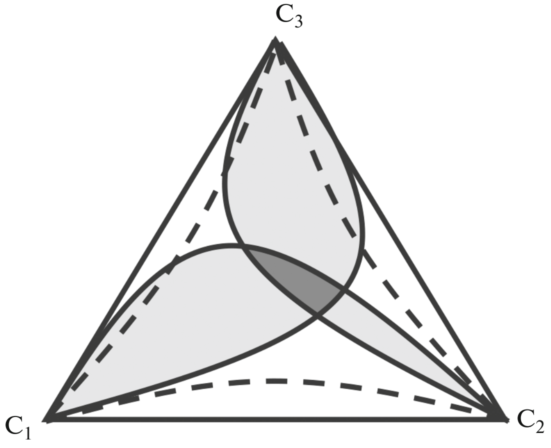

Fig. 1. Spinodal instability regions for two components in the state diagram of a three-component alloy (schematic view). Dashed lines correspond to the temperature T_1, when the spinodal decomposition areas do not overlap. Solid lines correspond to lower temperature $T_2 < T_1$, at which the overlap of spinodal regions is realized.

[29, 30], and Al–(Sc,Zr) [31–33]. In the present work, we provide a concise overview of recent findings derived from theoretical investigations into these alloys, preceded by discussion of the general conditions conducive to the formation of metastable disperse precipitates.

2. FORMATION CONDITIONS OF THE PRECIPITATES WITH CORE–SHELL STRUCTURE

There are two main scenarios of decomposition in alloys: according to the classical mechanism of nucleation and growth of new phase precipitates, and spinodal decomposition. Since the appearance of new phase nuclei requires thermal activation, the new phase is formed heterogeneously, at grain boundaries and other lattice defects. Therefore, the spinodal decomposition mechanism is preferred for the formation of disperse heterogeneous state, when nuclei of a new phase are formed in the grain volume spontaneously or with the activation energy $\Delta E \sim kT$ [34].

At the intermediate stage of spinodal decomposition, a highly disperse state is formed, which can be 'frozen' by rapid cooling. The Fe–Cr and Fe–Cu binary alloys are well-known examples of the implementation of such a mechanism [35]. Note that in the Fe–Cu alloy, spinodal decomposition commences in α-Fe with the formation of α-Cu nanoprecipitates, whose BCC lattice is rearranged into FCC when the critical size is reached [36].

The spinodal decomposition pattern in a three-component alloy is typically quite complex, since it is determined by the convexity of the free energy function along the spectrum of possible directions in the state diagram. In general, the spinodal decomposition of a three-component alloy was considered in [37, 38]. Figure 1 illustrates a particular case of the state diagram for a three-component alloy in presence of a decomposition stimulus affecting all components (i.e., the interaction energy between atoms of α and β varieties, $v_{\alpha\beta} < 0$). Should the figurative point of the alloy be situated within the region of overlapping spinodal regions (depicted in dark areas on the diagram), the expectation is that spinodal instability will manifest itself on different component pairs. In this case, it is conceivable that the precipitates of one component may stimulate the nucleation or impede the growth of the precipitates of another component, leading to an increase in alloy dispersion [7].

A common feature of various scenarios of spinodal decomposition is the coarsening of the microstructure during the ageing process, which is caused by the coalescence of precipitates. Nevertheless, even at elevated temperatures, this process can be decelerated or even halted entirely by the loss of lattice coherence, the segregation of phases at phase interfaces, or the precipitations of new phases during decomposition.

The theory of grain boundary segregation predicts that anomalous kinetics of grain growth and the appearance of equilibrium grain size if the segregation energy is higher (in modulus) than some critical value [39]. This effect was validated experimentally and by numerical simulations [24, 25]. The concepts of reference [39] can be applied to the analysis of segregation at phase interfaces. In [40], Monte Carlo simulation of alloy decomposition has demonstrated the possibility of forming equilibrium dispersive states due to the segregation of impurities at the phase interface. Moreover, the average size of the precipitates could decrease during evolution.

3. DECELERATION OF THE PRECIPITATE GROWTH AT THE STAGE OF COALESCENCE

The conditions of kinetic stabilization of precipitates during spinodal decomposition in a three-component alloy were considered in detail in [41]. Figure 2 shows the situation when the decomposition leads to the formation of the core–shell structure (time is given in dimensionless units, $\tau = tD_{\mathrm{A}}^{(\mathrm{M})}/L^2$, where t is time, $D_{\mathrm{A}}^{(\mathrm{M})}$ is the diffusion coefficient of atoms of variety A in the matrix (M), and L is the size of the simulation domain). From a thermodynamic perspective, the atoms of A and B varieties both exhibit tendencies towards decomposition. This is observed both within the matrix and in relation to one another, with all energies $v_{\alpha\beta} < 0$. Concurrently, component B exhibits adequate mobility within the precipitate volume A yet minimal mobility within the matrix (M). At temperatures below the critical point, the overlap of spinodal

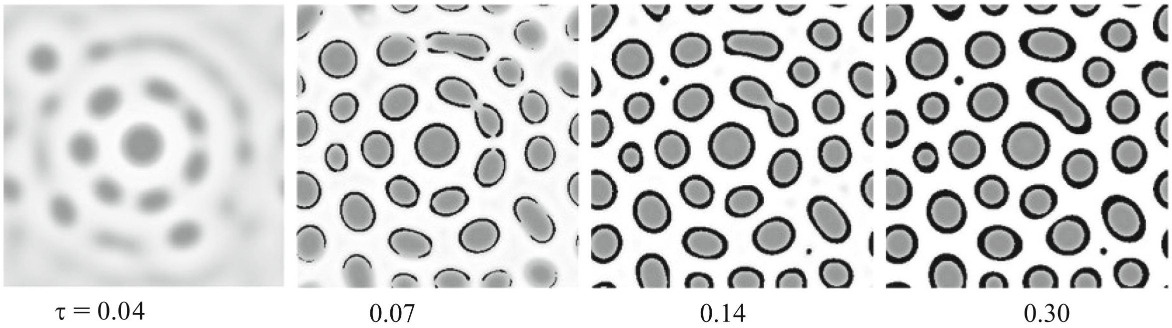

Fig. 2. Spinodal decomposition kinetics over component A and the formation of a "locking" shell enriched with a low-mobility component B [41].

regions is achieved (see Fig. 1), resulting in the decomposition with the participation of component A and the displacement of component B from the precipitates into the matrix.

"Locking" shell around the precipitates of component A (Fig. 2) represents a phase of intermediate composition A–B and is formed under the assumption of the concentration dependence of the mixing energy v_{BM} [41]. In the absence of this dependence, secondary precipitates of component B ('discontinuous shell') are formed around the primary separation of component A, which, at the appropriate ratio of diffusion coefficients, can also stabilize the disperse state.

Figure 3 shows the time dependent maximum size of precipitate of the component A in the case of continuous shell formation at different ratios of diffusion coefficients ($D_{\mathrm{A}}^{(\mathrm{M,shell})}$, $D_{\mathrm{B}}^{(\mathrm{M,A})}$ are the intrinsic diffusion coefficients of component A in the matrix and shell, and component B in the matrix and precipitates of component A, respectively, which were assumed in [41] to be equal to the corresponding isotopic diffusion coefficients). It can be observed that the decomposition process develops most rapidly when the diffusion of component B is completely frozen (curve *1*). The redistribution of component B results in the formation of a shell, which retards the decomposition by component A (compare curves *1* and *2*). At the same time, the most effective stabilization of precipitates is achieved if the mobility of component A decreases in the region of the formed shell (curve *3*), i.e., precipitates of component A are actually isolated from the matrix.

It should be noted that in the considered case the shell formation is energetically favorable, while the stability of the formed structure has rather kinetic reasons. Another scenario of kinetic stabilization is possible, when a non-equilibrium shell enriched with component B is formed around the precipitate, but without phase formation. Such a case is apparently implemented in the Al–Zr–Sc alloy [31] and will be discussed below.

4. SIMULATION RESULTS

4.1. Stability of Guinier–Preston Zones and θ'-Phase Precipitates in Al–Cu–X Alloys

The high strength of aluminum alloys is achieved as a result of the formation of nanoscale precipitates during annealing at moderate temperatures. The application of modern methods of first-principles simulation has facilitated an understanding of the processes occurring at the early stages of decomposition, as well as the formation of pre-precipitates in Al–Cu–X alloys (Guinier–Preston zones, GPZ [15]). The formation of GPZs in the form of plates parallel to {100} of the matrix can be attributed to the minimization of elastic stresses [5, 14]. From an alloy theory perspective, this phenomenon can be consistently accounted for by the contribution of multiparticle interactions [42]. The annealing of Al–Cu alloys at temperatures above room temperature results in the growth of GPZs

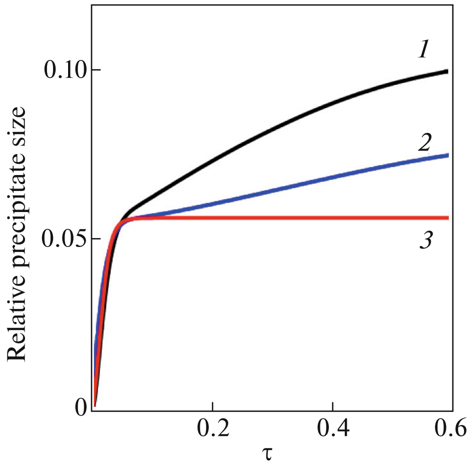

Fig. 3. Evolution of the maximum precipitate size of component A (with respect to the size of the computational domain *L*) [41]: (*1*) at $D_{\mathrm{B}}^{(\mathrm{M,A})} = 0$ (the shell is not formed); (*2*) $D_{\mathrm{B}}^{(\mathrm{M})} \ll D_{\mathrm{A}}^{(\mathrm{M})}$, $D_{\mathrm{A}}^{(\mathrm{shell})} = D_{\mathrm{A}}^{(\mathrm{M})} = D_{\mathrm{B}}^{(\mathrm{A})}$; (*3*) $D_{\mathrm{B}}^{(\mathrm{M})} \ll D_{\mathrm{A}}^{(\mathrm{M})}$, $D_{\mathrm{A}}^{(\mathrm{shell})} \ll D_{\mathrm{A}}^{(\mathrm{M})}$, $D_{\mathrm{B}}^{(\mathrm{A})} \ll D_{\mathrm{A}}^{(\mathrm{M})}$.

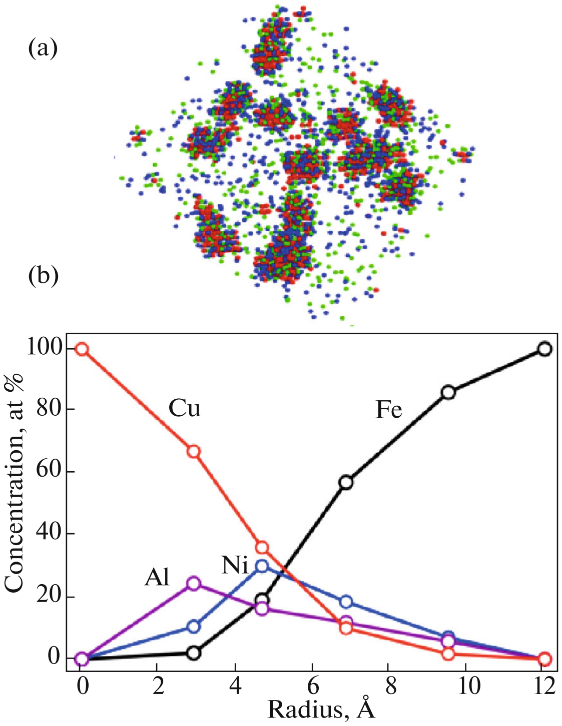

Fig. 4. Precipitates formed in BCC–Fe after 1.5×10^5 MD + MC steps at $T = 775$ K (a). The red color corresponds to Cu, blue—to Ni, and green—to Al. Distribution of atoms along the precipitate radius (b). (MD + MC—Molecular Dynamics + Monte Carlo simulation.)

and their rearrangement in accordance with the following scheme: GPZ I (comprising a single layer of Cu atoms) → θ''(GPZ II) → θ'-phase → θ-phase [5]. This process results in the coarsening of the precipitates and a concomitant deterioration of the strength properties.

Recently, Al–Cu alloys containing Mn or Zr have been presented, whose additives allowed stabilizing the fine structure of θ'-precipitates up to rather high temperatures [27, 44]. High-resolution electron microscopy revealed the presence of segregations of Mn and Zr at the boundary of θ'-precipitates with the matrix [44]. An explanation of this phenomenon based on the results of ab initio calculations was proposed in [27].

A sequential ab initio calculation of the interaction of alloying elements with the coherent boundary of θ'-precipitates in Al–Cu-based alloy was conducted in [28]. The results revealed that the θ'-precipitate boundary half-filled with Cu atoms is the most energetically preferable, and it is exactly such a boundary that is formed according to the rearrangement mechanism θ''(GPZ II) → θ'-phase, proposed in [45]. It is shown that the peculiarities of chemical bonding determine the interactions of alloying elements with the coherent boundary of the θ'-phase. The value of the calculated interaction energies for elements with closed (Cu, Zn) or unfilled (Mg, Si) *d*-electron shell is small (<–0.1 eV) in comparison with transition *d*-metals (Mn, Zr), for which it is approximately –0.3 eV.

Thus, the results of ab initio simulation [27, 28] demonstrate that doping by Mn or Zr will lead to the formation of segregations at the θ' phase boundary. However, the question of whether these segregations are sufficient to prevent the growth of θ'-precipitates remains open and requires further investigation.

4.2. Decomposition Kinetics and Stability of Precipitates in Fe–Cu–(Ni, Al) Alloys

Copper is the sole alloying element in steel that exhibits a proclivity for clustering [35, 46]. The formation of BCC–Cu nanoscale precipitates within the α-Fe matrix in the Fe–Cu system results in the attainment of high strength properties while maintaining ductility [19, 47, 48].

The decomposition kinetics of supersaturated Fe–Cu–Ni–Al solid solutions has been investigated in detail experimentally. In low-carbon steels alloyed with Cu, Ni, Al, and Mn very high strength of about 1600 MPa can be obtained after aging at 500–550°C for 1–2 hours [49]. The microstructure of Fe–Cu–Ni–Al–Mn alloys with different total content of alloying elements was investigated in [50, 51]. It is shown that high strength properties of the alloy with low content of alloying elements are conditioned by the formation of Cu particles, whose surface is enriched in Ni and Al atoms (co-precipitation mode [3]). With an increase in the Ni and Al content, the kinetics of decomposition changes, resulting in the formation of precipitate particles based on Cu and the *B*2 NiAl intermetallic compound as a result of aging.

The decomposition and formation of precipitates in BCC alloys of Fe–Cu–Ni and Fe–Cu–Mn were investigated in [30] by statistical Monte Carlo simulation with first-principles effective interatomic interactions. The results have demonstrated that Ni promotes the formation of Cu precipitates and segregates to the Cu/Fe interfacial surface, while Mn has no significant effect on the decomposition.

In [52, 53], a complex MD + MC approach, which includes Monte Carlo and molecular dynamic simulation, was employed to investigate the kinetics of the precipitates formation in a Fe–1.5 at % Cu–2.0 at % Ni–1.5 at % Al multicomponent low-doped alloy. It has been demonstrated that during the annealing process, a layer comprising a high concentration of Al and Ni atoms forms on the surface of Cu nanoparticles (Fig. 4).

As shown in [52], the decomposition of the alloy commences with the formation of Cu clusters. Despite the higher diffusion coefficient of Al and Ni atoms in the BCC–Fe matrix, the formation of clusters enriched in Ni and Al atoms does not occur. The formation of NiAl particle nuclei should be anticipated in alloys exhibiting a markedly elevated Ni content. For Fe–Cu–Ni–Al alloys with a close content of Cu, Ni, and Al, the decisive factor is the interaction energy between Cu atoms, which significantly exceeds the energies of other types of interaction and determines the high driving force causing the formation of precipitates.

The formation of a shell comprising Ni and Al atoms inhibits the growth of Cu particles. As a result, the formation of Cu nanoparticles of a considerably smaller size is observed in the Fe–Cu–Ni–Al alloy in comparison to the binary alloy. Thus, the addition of Ni and Al to the Fe–Cu alloy, even in trace amounts, impedes the growth of Cu particles. This is due to the formation of a protective shell and the activation of a mechanism analogous to that described in Section 2.

4.3. Non-Equilibrium Core–Shell Structures in Al–Sc–Zr Alloys

Alloying with Sc is another known way to increase the strength properties of Al alloys. The formation of nanoscale coherent Al_3Sc precipitates with $L1_2$ superstructure significantly increases the strength of Al alloys at temperatures up to 300°C [21, 55, 56]. However, further increase in temperature results in a rapid coarsening of precipitates and loss of strength properties. The introduction of Zr as a microalloying element results in the formation of $Al_3(Sc_XZr_{1-X})$ nanoparticles. As a result, the alloy exhibits high strength properties up to temperatures of ~500°C. According to the existing views, the increase in precipitate stability is due to the formation of a distinctive precipitate structure comprising a predominantly Sc-containing core and a Zr-enriched shell [32, 57, 58].

The formation of precipitates during annealing in a supersaturated Al–Sc–Zr solid solution was investigated through kinetic Monte Carlo simulation using ab initio calculated interatomic potentials [31]. The simulation results have revealed a clear tendency towards the formation of a Zr-enriched shell. However, they did not allow for a conclusion to be drawn regarding the stabilization mechanism of precipitates, especially at the stage of coalescence. Moreover, as it was found experimentally [32], the structure of $Al_3(Sc_XZr_{1-X})$ precipitates is quite complex and is characterized by notable heterogeneity in the distribution of both Zr and Sc, which is not reproduced by the model [31].

A more consistent approach, based on the statistical theory of alloys with the first-principle parametrization of interatomic interactions was used in [33] to simulate both the formation of precipitates and their dissolution. It was shown that the core–shell structure is formed in a certain range of parameters and is very sensitive to the details of the diffusion mechanism in the alloy.

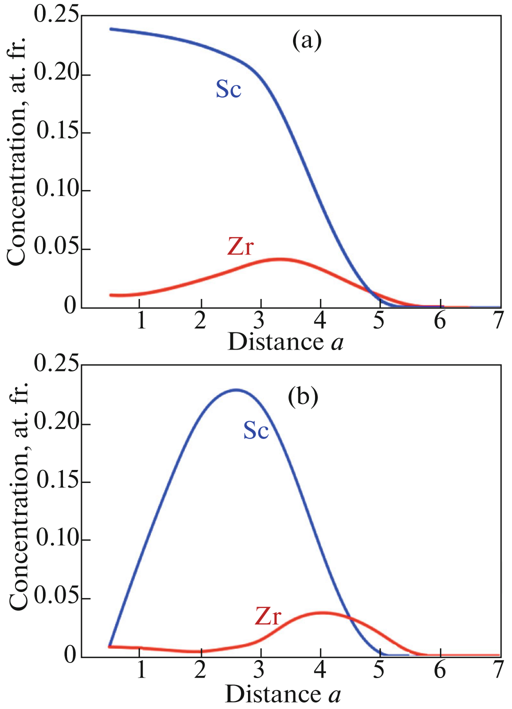

Fig. 5. Averaged local concentration of Sc and Zr formed during annealing at $T = 800$ K as a function of the distance to the center of the precipitate (*a*—lattice parameter) [33]. In fragments (a) and (b) all parameters are the same with the exception for Γ_2—exchange frequency of atoms of the second neighbors, which is 10 times more in fragment (a) in comparison with (b).

The diffusion mechanism in an ordered $L1_2$ particle is complex, and the diffusion process, which leads to the exchange of first neighbors, is energetically impeded because it causes the order-disorder transformation. Accordingly, in reference [33], the interchange of atoms occupying the positions of both first and second neighbors was contemplated.

As can be seen from the results shown in Fig. 5a, with increased exchange frequencies over the second neighbors Γ_2, the usual core–shell structure is formed. At the same time, a decrease in the frequency of Γ_2 radically changes the pattern (Fig. 5b): thus, stratification is observed inside the particle, both in scandium and zirconium. It is precisely this structure of precipitates that has been observed experimentally [32].

The simulation conducted in [33] has demonstrated that the presence of a Zr-enriched shell impedes the dissolution of minor precipitates, thereby inhibiting the coarsening of the structure. Consequently, the formation of the particle structure of the core–shell type significantly alters the evolution of the ensemble of precipitates during annealing, enhancing their thermal stability.

CONCLUSIONS

The implementation of metastable dispersed states is a common practice in the production of alloys, since it allows for the attainment of high strength properties while maintaining sufficient ductility. Among the processes that result in the formation of these states, the formation of precipitate particles with a core–shell structure occupies a special place. This requires the fulfillment of specific conditions (Section 2), providing energetically advantageous formation of the disperse state. The stability of the resulting structure is typically determined by kinetic factors (Section 3) and the presence of a shell (in the form of a phase layer of intermediate composition), which prevents the coarsening of the structure at the coalescence stage. The results of atomistic simulation testify to the implementation of exactly such a mechanism in Fe–Cu–(Ni,Al) and Al–Sc–Zr alloys. At the same time, in the Al–Cu–X system the increased stability of θ'-phase is attained as a consequence of the change of surface energy due to the formation of segregations.

FUNDING

The study was conducted in accordance with the state assignment of the Ministry of Education and Science of the Russian Federation (theme "Structure" AAAA-A18-118020190116-6).

CONFLICT OF INTEREST

The authors of this work declare that they have no conflicts of interest.

OPEN ACCESS

REFERENCES

1. H. Gleiter, "Nanostructured materials: Basic concepts and microstructure," Acta Mater. **48**, 1–29 (2000). https://doi.org/10.1016/s1359-6454(99)00285-2
2. R. Z. Valiev, A. P. Zhilyaev, and T. G. Langdon, *Bulk Nanostructured Materials: Fundamentals and Application* (Wiley, Hoboken, NJ, 2014).
3. Z. B. Jiao, J. H. Luan, M. K. Miller, Y. W. Chung, and C. T. Liu, "Co-precipitation of nanoscale particles in steels with ultra-high strength for a new era," Mater. Today **20**, 142–154 (2017). https://doi.org/10.1016/j.mattod.2016.07.002
4. Q. Jiang and C. C. Yang, "Size effect on the phase stability of nanostructures," Curr. Nanosci. **4**, 179–200 (2008). https://doi.org/10.2174/157341308784340949
5. Yu. N. Gornostyrev and M. I. Katsnelson, "Misfit stabilized embedded nanoparticles in metallic alloys," Phys. Chem. Chem. Phys. **17**, 27249–27257 (2015). https://doi.org/10.1039/c5cp04641f
6. S. Chakrabarty and Z. Nussinov, "Modulation and correlation lengths in systems with competing interactions," Phys. Rev. B **84**, 144402 (2011). https://doi.org/10.1103/physrevb.84.144402
7. A. Deschamps and C. R. Hutchinson, "Precipitation kinetics in metallic alloys: Experiments and modeling," Acta Mater. **220**, 117338 (2021). https://doi.org/10.1016/j.actamat.2021.117338
8. A. J. Bray, "Theory of phase-ordering kinetics," Adv. Phys. **43**, 357–459 (1994). https://doi.org/10.1080/00018739400101505
9. R. Bručas, H. Hafermann, M. I. Katsnelson, I. L. Soroka, O. Eriksson, and B. Hjörvarsson, "Magnetization and domain structure of bcc $Fe_{81}Ni_{19}Co$ (001) superlattices," Phys. Rev. B **69**, 064411 (2004). https://doi.org/10.1103/PhysRevB.69.064411
10. J. Lyubina, B. Rellinghaus, O. Gutfleisch, and M. Albrecht, "Structure and magnetic properties of L10-ordered Fe–Pt alloys and nanoparticles," in *Handbook of Magnetic Materials*, Ed. by K. H. J. Buschow (Elsevier, Amsterdam, 2011), Vol. 19, pp. 291–407. https://doi.org/10.1016/b978-0-444-53780-5.00005-3
11. V. I. Levitas and D. L. Preston, "Thermomechanical lattice instability and phase field theory of martensitic phase transformations, twinning and dislocations at large strains," Phys. Lett. A **343**, 32–39 (2005). https://doi.org/10.1016/j.physleta.2005.05.034
12. V. A. Levin, V. I. Levitas, K. M. Zingerman, and E. I. Freiman, "Phase-field simulation of stress-induced martensitic phase transformations at large strains," Int. J. Solids Struct. **50**, 2914–2928 (2013). https://doi.org/10.1016/j.ijsolstr.2013.05.003
13. W. C. Leslie and E. Hornbogen, "Physical metallurgy of steels," in *Physical Metallurgy*, Ed. by R. W. Cahn and P. Haasen, 4th ed. (Elsevier, Amsterdam, 1996), Vol. 2, pp. 1555–1620. https://doi.org/10.1016/b978-044489875-3/50022-3
14. A. G. Khachaturyan, *Theory of Structural Transformations in Solids* (Wiley, New York, 1983).
15. A. Guinier, "Structure of age-hardened aluminium–copper alloys," Nature **142**, 569–570 (1938). https://doi.org/10.1038/142569b0
16. G. D. Preston, "The diffraction of X-rays by age-hardening aluminium copper alloys," Proc. R. Soc. London, Ser. A **167**, 526–538 (1938). https://doi.org/10.1098/rspa.1938.0152

17. E. W. Collings, *The Physical Metallurgy of Titanium Alloys* (ASM, Metals Park, OH, 1984).
18. H. Kubo and S. Farjami, "Nucleation of athermal omega phase in Cu–Zn system," Mater. Sci. Eng., A **438–440**, 181–185 (2006). https://doi.org/10.1016/j.msea.2005.12.074
19. M. E. Fine, J. Z. Liu, and M. D. Asta, "An unsolved mystery: The composition of bcc Cu alloy precipitates in bcc Fe and steels," Mater. Sci. Eng., A **463**, 271–274 (2007). https://doi.org/10.1016/j.msea.2006.07.164
20. H. Rösner, Ch. T. Koch, and G. Wilde, "Strain mapping along Al–Pb interfaces," Acta Mater. **58**, 162–172 (2010). https://doi.org/10.1016/j.actamat.2009.08.065
21. J. Røyset and N. Ryum, "Scandium in aluminium alloys," Int. Mater. Rev. **50**, 19–44 (2005). https://doi.org/10.1179/174328005X14311
22. T. V. Zaporozhets, O. N. Podolyan, and A. M. Gusak, "Growth kinetics of nanoshells of the intermediate phase with allowance for finite reaction rates at interphase boundaries," Phys. Met. Metallogr. **115**, 268–276 (2014). https://doi.org/10.1134/s0031918x14030120
23. M. Nastar, L. T. Belkacemi, E. Meslin, and M. Loyer-Prost, "Thermodynamic model for lattice point defect-mediated semi-coherent precipitation in alloys," Commun. Mater. **2**, 32 (2021). https://doi.org/10.1038/s43246-021-00136-z
24. J. R. Trelewicz and Ch. A. Schuh, "Grain boundary segregation and thermodynamically stable binary nanocrystalline alloys," Phys. Rev. B **79**, 094112 (2009). https://doi.org/10.1103/physrevb.79.094112
25. P. C. Millett, R. P. Selvam, and A. Saxena, "Stabilizing nanocrystalline materials with dopants," Acta Mater. **55**, 2329–2336 (2007). https://doi.org/10.1016/j.actamat.2006.11.028
26. P. Sharma and S. Ganti, "Size-dependent Eshelby's tensor for embedded nano-inclusions incorporating surface/interface energies," J. Appl. Mech. **71**, 663–671 (2004). https://doi.org/10.1115/1.1781177
27. A. Shyam, S. Roy, D. Shin, J. D. Poplawsky, L. F. Allard, Y. Yamamoto, J. R. Morris, B. Mazumder, J. C. Idrobo, A. Rodriguez, T. R. Watkins, and J. A. Haynes, "Elevated temperature microstructural stability in cast AlCuMnZr alloys through solute segregation," Mater. Sci. Eng., A **765**, 138279 (2019). https://doi.org/10.1016/j.msea.2019.138279
28. M. V. Petrik, Yu. N. Gornostyrev, and P. A. Korzhavyi, "Segregation of alloying elements to stabilize θ' phase interfaces in Al–Cu based alloys," Scr. Mater. **202**, 114006 (2021). https://doi.org/10.1016/j.scriptamat.2021.114006
29. R. Prakash Kolli and D. N. Seidman, "The temporal evolution of the decomposition of a concentrated multicomponent Fe–Cu-based steel," Acta Mater. **56**, 2073–2088 (2008). https://doi.org/10.1016/j.actamat.2007.12.044
30. O. I. Gorbatov, Yu. N. Gornostyrev, P. A. Korzhavyi, and A. V. Ruban, "Effect of Ni and Mn on the formation of Cu precipitates in α-Fe," Scr. Mater. **102**, 11–14 (2015). https://doi.org/10.1016/j.scriptamat.2015.01.016
31. E. Clouet, L. Laé, T. Epicier, W. Lefebvre, M. Nastar, and A. Deschamps, "Complex precipitation pathways in multicomponent alloys," Nat. Mater. **5**, 482–488 (2006). https://doi.org/10.1038/nmat1652
32. A. Orthacker, G. Haberfehlner, J. Taendl, M. C. Poletti, B. Sonderegger, and G. Kothleitner, "Diffusion-defining atomic-scale spinodal decomposition within nanoprecipitates," Nat. Mater. **17**, 1101–1107 (2018). https://doi.org/10.1038/s41563-018-0209-z
33. A. Yu. Stroev, O. I. Gorbatov, Yu. N. Gornostyrev, and P. A. Korzhavyi, "Ab-initio based modeling of precipitation in Al–(Sc,Zr) alloy. Formation and stability of a core–shell structure," Comput. Mater. Sci. **218**, 111912 (2023). https://doi.org/10.1016/j.commatsci.2022.111912
34. K. Binder and P. Fratzl, "Spinodal decomposition," in *Phase Transformations in Materials*, Ed. by G. Kostorz (Wiley, Weinheim, 2001), pp. 409–480. https://doi.org/10.1002/352760264x.ch6
35. O. I. Gorbatov, I. K. Razumov, Yu. N. Gornostyrev, V. I. Razumovskiy, P. A. Korzhavyi, and A. V. Ruban, "Role of magnetism in Cu precipitation in α-Fe," Phys. Rev. B **88**, 174113 (2013). https://doi.org/10.1103/PhysRevB.88.174113
36. A. Deschamps, M. Militzer, and W. J. Poole, "Precipitation kinetics and strengthening of a Fe–0.8 wt % Cu alloy," ISIJ Int. **41**, 196–205 (2001). https://doi.org/10.2355/isijinternational.41.196
37. J. E. Morral and J. W. Cahn, "Spinodal decomposition in ternary systems," Acta Metall. **19**, 1037–1045 (1971). https://doi.org/10.1016/0001-6160(71)90036-8
38. L.-Q. Q. Chen, "Computer simulation of spinodal decomposition in ternary systems," Acta Metall. Mater. **42**, 3503–3513 (1994). https://doi.org/10.1016/0956-7151(94)90482-0
39. J. Weissmüller, "Alloy effects in nanostructures," Nanostruct. Mater. **3**, 261–272 (1993). https://doi.org/10.1016/0965-9773(93)90088-s
40. I. K. Razumov, "Anomalous dispersed states of alloys caused by segregation of impurities at phase interfaces," Phys. Solid State **56**, 780–784 (2014). https://doi.org/10.1134/s1063783414040283
41. I. K. Razumov and Yu. N. Gornostyrev, "Metastable dispersed states arising upon three-component alloy decomposition," Phys. Solid State **61**, 2493–2502 (2019). https://doi.org/10.1134/s1063783419120436
42. O. I. Gorbatov, Yu. N. Gornostyrev, and P. A. Korzhavyi, "Many-body mechanism of Guinier–Preston zones stabilization in Al–Cu alloys," Scr. Mater. **138**, 130–133 (2017). https://doi.org/10.1016/j.scriptamat.2017.05.044
43. K. Kim, A. Roy, M. P. Gururajan, C. Wolverton, and P. W. Voorhees, "First-principles/phase-field modeling of θ' precipitation in Al–Cu alloys," Acta Mater. **140**, 344–354 (2017). https://doi.org/10.1016/j.actamat.2017.08.046

44. D. Shin, A. Shyam, S. Lee, Yu. Yamamoto, and J. A. Haynes, "Solute segregation at the Al/θ'–Al_2Cu interface in Al–Cu alloys," Acta Mater. **141**, 327–340 (2017). https://doi.org/10.1016/j.actamat.2017.09.020
45. M. V. Petrik, Y. N. Gornostyrev, and P. A. Korzhavyi, "Point defect interactions with Guinier–Preston zones in Al–Cu based alloys: Vacancy mediated GPZ to θ'-phase transformation," Scr. Mater. **165**, 123–127 (2019). https://doi.org/10.1016/j.scriptamat.2019.02.024
46. O. I. Gorbatov, A. H. Delandar, Yu. N. Gornostyrev, A. V. Ruban, and P. A. Korzhavyi, "First-principles study of interactions between substitutional solutes in bcc iron," J. Nucl. Mater. **475**, 140–148 (2016). https://doi.org/10.1016/j.jnucmat.2016.04.013
47. S. Vaynman, R. S. Guico, M. E. Fine, and S. J. Manganello, "Estimation of atmospheric corrosion of high-strength, low-alloy steels," Metall. Mater. Trans. A **28**, 1274–1276 (1997). https://doi.org/10.1007/s11661-997-0294-0
48. D. Isheim, R. P. Kolli, M. E. Fine, and D. N. Seidman, "An atom-probe tomographic study of the temporal evolution of the nanostructure of Fe–Cu based high-strength low-carbon steels," Scr. Mater. **55**, 35–40 (2006). https://doi.org/10.1016/j.scriptamat.2006.02.040
49. M. Kapoor, D. Isheim, G. Ghosh, S. Vaynman, M. E. Fine, and Y.-W. Chung, "Aging characteristics and mechanical properties of 1600MPa body-centered cubic Cu and B2-NiAl precipitation-strengthened ferritic steel," Acta Mater. **73**, 56–74 (2014). https://doi.org/10.1016/j.actamat.2014.03.051
50. M. Kapoor, D. Isheim, S. Vaynman, M. E. Fine, and Y.-W. Chung, "Effects of increased alloying element content on NiAl-type precipitate formation, loading rate sensitivity, and ductility of Cu- and NiAl-precipitation-strengthened ferritic steels," Acta Mater. **104**, 166–171 (2016). https://doi.org/10.1016/j.actamat.2015.11.041
51. Z. B. Jiao, J. H. Luan, M. K. Miller, and C. T. Liu, "Precipitation mechanism and mechanical properties of an ultra-high strength steel hardened by nanoscale NiAl and Cu particles," Acta Mater. **97**, 58–67 (2015). https://doi.org/10.1016/j.actamat.2015.06.063
52. I. N. Kar'kin, L. E. Kar'kina, Yu. N. Gornostyrev, and A. P. Korzhavyi, "Kinetics of early decomposition stages in diluted bcc Fe–Cu–Ni–Al alloy: MC+MD simulation," Phys. Solid State **61**, 601–608 (2019). https://doi.org/10.1134/s1063783419040152
53. I. N. Karkin, L. E. Karkina, Yu. N. Gornostyrev, and P. A. Korzhavyi, "Effect of Ni and Al on the decomposition kinetics and stability of Cu-enriched precipitates in Fe–Cu–Ni–Al alloys: Results of MD + MC simulation," Phys. Met. Metallogr. **122**, 498–503 (2021). https://doi.org/10.1134/s0031918x21050045
54. Z. B. Jiao, J. H. Luan, M. K. Miller, C. Y. Yu, and C. T. Liu, "Group precipitation and age hardening of nanostructured Fe-based alloys with ultra-high strengths," Sci. Rep. **6**, 21364 (2016). https://doi.org/10.1038/srep21364
55. B. A. Chen, L. Pan, R. H. Wang, G. Liu, P. M. Cheng, L. Xiao, and J. Sun, "Effect of solution treatment on precipitation behaviors and age hardening response of Al–Cu alloys with Sc addition," Mater. Sci. Eng., A **530**, 607–617 (2011). https://doi.org/10.1016/j.msea.2011.10.030
56. L. I. Kaigorodova, I. G. Brodova, E. I. Sel'nikhina, and O. R. Shamsheeva, "Effect of small additions of Sc and Zr on the fine structure of Al–Zn–Mg–Cu alloy after rapid solidication and high-temperature annealing," Phys. Met. Metallogr. **90**, 281–287 (2000).
57. P. W. Voorhees, "Scandium overtakes zirconium," Nat. Mater. **5**, 435–436 (2006). https://doi.org/10.1038/nmat1663
58. O. N. Senkov, M. R. Shagiev, S. V. Senkova, and D. B. Miracle, "Precipitation of Al_3(Sc,Zr) particles in an Al–Zn–Mg–Cu–Sc–Zr alloy during conventional solution heat treatment and its effect on tensile properties," Acta Mater. **56**, 3723–3738 (2008). https://doi.org/10.1016/j.actamat.2008.04.005